JOURNAL OF SOLID STATE CHEMISTRY **123,** 191–202 (1996)
ARTICLE NO. 0168

Effect of Mechanical Activation on the Real Structure and Reactivity of Iron (III) Oxide with Corundum-Type Structure

V. A. Sadykov,[1] L. A. Isupova, S. V. Tsybulya, S. V. Cherepanova, G. S. Litvak, E. B. Burgina, G. N. Kustova, V. N. Kolomiichuk, V. P. Ivanov, E. A. Paukshtis, A. V. Golovin, and E. G. Avvakumov

Boreskov Institute of Catalysis, Siberian Division, Russian Academy of Sciences, Pr. Lavrentieva, 5, 630090 Novosibirsk, Russia; and Institute of Solid State Chemistry and Mineral Processing, Siberian Division, Russian Academy of Sciences, Ul. Dierzhavina 18, 630091 Novosibirsk, Russia

Received May 25, 1995; in revised form January 16, 1996; accepted January 17, 1996

For highly dispersed α-Fe_2O_3 the effect of mechanical activation in the high-powered ball mill under Ar atmosphere on its real structure and reactivity has been studied by using methods sensitive to the bulk (X-ray diffraction, TEM, IR spectroscopy of the lattice vibrations, static magnetic method) as well as to surface properties (SIMS, IR spectroscopy of adsorbed CO and surface hydroxyls, catalytic CO oxidation). Before activation, initial sample was shown to have a rather high density of surface and near-surface extended defects with local spinel structure probably stabilized by admixed sodium ions, while the bulk is free from such disturbances. Cooperative distortion of the lattice (increase of the distance between cation layers and some equalizing of the O–O distances in the anion sublattice) was observed and explained by an effect of the admixed sodium cations in the interstitial positions. Mechanical activation was found to generate anion vacancies in the bulk that was accompanied by a further increase of the distance between cation layers, whereas a mode of relaxation within the anion layers approaches that typical for the perfect hematite. A fall of the density of near-surface extended defects caused by mechanical activation was explained by the glide and/or climb mechanisms and was found to correlate with the decrease of the hematite reactivity.

INTRODUCTION

Real (defect) structure of solids is known to influence substantially their reactivity in both solid state reactions and heterogeneous catalysis (1–3). However, yet little is known in details about the relative abundance and importance of the various types of defects (point, extended) for dispersed oxide systems. Recently (4–9) we have undertaken studies of powdered transition metal oxides to elucidate the atomic arrangement of the surface centers which determine catalytic activity in oxidation reactions, their relation to bulk defects being of special interest. Oxides of spinel and corundum types appear to be the most promising objects since previous consideration of structures of the basic types of bulk extended defects by Kronberg (10), Hornstra (11) and Bursill and Withers (12) have made it possible to use X-ray powder diffraction data to estimate their densities. Earlier (8–9) real structure of α-Fe_2O_3 samples prepared by thermal decomposition of needle-like goethite (α-FeOOH) and then calcined at 400–1100°C has been investigated by transmission electron microscopy (TEM), X-ray powder diffraction (XPD), and IR spectroscopy of lattice vibrations. In the low-temperature samples (annealing temperatures $\leq$500°C) extended defects such as twins and stacking faults located in the basal plane and generated in the course of topotactical goethite–hematite transformation dominate. Besides, cooperative distortions of the hematite lattice assigned to effect of residual hydroxyls were observed. At higher temperatures of annealing (up to 800–900°C) genetic defects disappear while new types of extended defects located in the rhombohedral and prismatic planes were generated by recrystallization. At temperatures around 1000–1100°C, all bulk extended defects are annealed while numerous surface extended defects emerge due to reconstruction of the prismatic faces.

To study the effect of the nature of the precursor on the particles morphology and predominant types of defects, a sample prepared via thermal decomposition of the ammonium oxalatoferriate $(NH_4)_3[Fe(C_2O_4)_3]\ 3H_2O$ was used as starting in this work. Defect structure of the sample was changed by mechanical activation followed by a rather soft thermal annealing. For fine powders this method allows to change bulk defects densities without substantially influencing the particles morphology (13). In this article the main efforts were focused on analysis of the linkage between surface and bulk defects as related to oxide reactivity. Surface defects were probed by using infrared spectroscopy of adsorbed CO known to be a very sensitive tool (7), while reactivity was characterized by the rate of carbon monoxide catalytic oxidation. Some earlier data (3) and our results (4, 14) favor great structural sensitivity of this

[1] To whom correspondence should be addressed.

0022-4596/96 $18.00

reaction when it is catalyzed by transition metal oxides. Moreover, recently we have obtained a rather good correlation between the specific catalytic activities of iron oxides and densities of surface defect centers—clusters of coordinatively unsaturated Fe^{2+} cations, the latter being estimated from the IR spectral data of adsorbed CO [15]. We hoped also to elucidate the main features of mechanical activation of finely powdered hematite, which are closely related to its defect structure. A rather unexpected effect of mechanical activation on cooperative distortions of the hematite lattice (8, 9) was observed and discussed.

EXPERIMENTAL

All effects of mechanical activation and subsequent annealing were studied on the sample of α-Fe_2O_3 prepared by air decomposition of ammonium oxalatoferriate. As judged from the XPD and magnetic susceptibility data, at an early state of decomposition an intermediate compound γ-Fe_2O_3 of the spinel structure was formed. After 10 hr of calcination at 400°C, ca. 40% of the γ-phase still remained. Air annealing for 24 hr at 500°C reduced the amount of this admixture to ca. 1% and this sample was subjected to mechanical activation. Henceforth this sample is referred to as ''initial.''

To estimate a possible share of this γ-phase admixture in the overall sample reactivity (in the case that we have here pure mechanical mixture), the same needle-like goethite as used previously (8, 9) was reduced at 400°C in the stream of hydrogen saturated by water vapor at room temperature, then annealed in He at the same temperature. Thus prepared Fe_3O_4 phase was then oxidized consequently in the flow of 1% CO + 1%O_2 in He at 500 K and 1% O_2 in He at 673 K into pure γ-Fe_2O_3 (5).

Mechanical activation was carried out in the Ar atmosphere under 40 g acceleration in an EI-2 × 150 planetary ball mill equipped with corundum drums and balls; the balls/oxide weight ratio was 50:1. The time of activation was varied from 1 to 15 min. Samples subjected to mechanical activation are henceforth referred to as ''activated.''

Electron microscopy. All the specimens were examined in a JEM-100 CX microscope. The resolution limit of the machine is about 3 Å, the accelerating potential 100 kV. Specimens were deposited onto a carbon film supported on a copper grid from ethanol slurry.

Thermal analysis of the samples was carried out using a Q-1500 device at a heating rate of 10°C/min in air or in a He stream.

XPD patterns were obtained with a URD-6 diffractometer (Germany) using CuK_β radiation. The scanning region 2θ was equal to 20°–90° with a step of 0.02°. The profile step counting time was 60 sec; the computer program system Polycrystall (16) was used to determine the structural parameters (atomic coordinates, occupation of positions, etc.). Particle sizes D were calculated with the Scherrer equation $D = k\lambda/\Delta(2\theta)\cos\theta$, where k is a constant equal to 0.9; λ is the X-ray wavelength used; $\Delta(2\theta)$ is the broadening of the diffraction peak chosen calculated from the expression $[\Delta(2\theta)]^2 = H^2_{\text{exp}} - H^2_{\text{std.}}$ (where H_{exp} and H_{std} are the half-widths of the specimen and standard substance, respectively); and θ is the diffraction angle of the peak maximum considered.

IR-spectra in the 200–1000 cm^{-1} region were obtained using M-80 spectrometer. The samples were prepared by dusting on the CsI supports.

Surface chemical composition was analyzed with SIMS method using MS-7201 mass spectrometer. The energy of the incident Ar^+ ion beam was equal to 4 KeV, the current density 10–20 mka/cm^2. To prevent sample charging during ion bombardment, samples were supported onto the high purity indium foil. In the experiments, the dependencies of Fe^+, O^+, Na^+, C^+, and Al^+ secondary ion currents on the incident beam fluence were measured.

Magnetic susceptibility was determined by Faraday method at room temperature.

Relative densities of extended defects were evaluated by the X-ray small angle scattering method (SAXS) (4). In these experiments Cu$K\alpha$ radiation with a nickel filter and an amplitude analyzer were used.

Infrared spectroscopy of surface hydroxyls and adsorbed CO. Wafers with densities of 16–18 mg/cm^2 were placed in an IR cell that allowed thermal treatment in controlled atmospheres and in vacuum. Samples were pretreated at 673 K in oxygen at 180 Torr for 1 hr (desorbed products of oxidation were frozen in a liquid nitrogen cooled trap) with subsequent cooling under oxygen to room temperature and evacuation up to 10^{-3} Torr. Spectra in OH stretching region (3000–3800 cm^{-1}) were recorded at room temperature; IR-spectra of adsorbed CO in the carbonyl stretching region were registered at 163 K and p_{CO} = 13 Torr. In these experiments UR-20 spectrometer was used and spectra analysis was carried out by using programs (17).

Sample reactivity was characterized by the rate of carbon monoxide catalytic oxidation in the mixture of 1%CO + 1% O_2 in He determined in the range of 413–500 K using a microreactor with the vibrofluidized bed of catalysts and pulse/flow kinetic installation (14). Before measurements, the samples were successively pretreated at 500 and 673 K in the flow of oxygen purified by passing through traps filled with CuO/alumina kept at 573 K, silica gel (298 K) and finally through traps cooled by liquid nitrogen. The rates were determined in essentially differential conditions (CO conversion <10%) and expressed as a number of CO molecules oxidized per square meter per second. When necessary, surface reduction of the samples by pulses of 1% CO in He was carried out in the same installation.

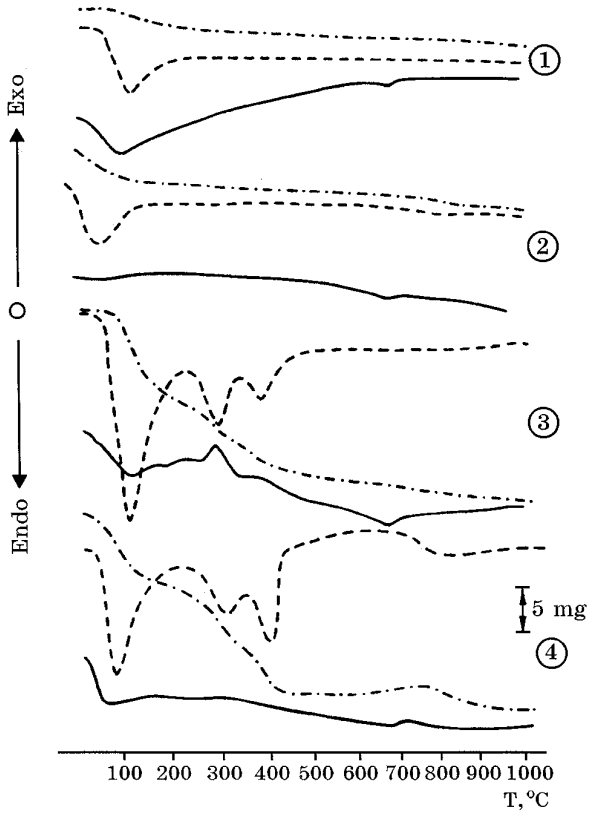

FIG. 1. DTA (solid lines), DTG (dashed lines), and TG (dashed–dotted lines) curves for initial (1, 2) and activated for 15 min (3, 4) samples of hematite. 1 and 3 are experiments carried out in air; 2 and 4 in He. Sample weights: 400 mg in 1, 2; 1000 mg in 3, 4.

Specific surface values were determined by BET method using Ar thermal desorption data.

RESULTS

Thermal Analysis

1. Initial sample. A broad intense endoeffect centered at 100°C and accompanied by a weight loss ca. 0.5% was observed in both air and He (Fig. 1, curves 1, 2). It is usually assigned to removal of adsorbed water. A weak endoeffect at 665°C without any change of weight is due to transition of α-Fe_2O_3 phase into the paramagnetic state (Néel temperature is around 936 K (18)).

2. Activated samples. As activation proceeds, exoeffects at 280°C and 370°C appear and grow, while endoeffect due to water removal increases. On DTG curves two new weight loss effects situated at ~280°C and ~390°C emerge. For sample activated 15 min these effects correspond to 0.3 and 1% decrease of weight (Fig. 1, curve 3, 4). DTA/DTG curves obtained in He stream differ from those recorded in air: in He exoeffects are hardly visible while weight losses are somewhat enhanced (Fig. 1, curve 4). In the same temperature region DTG peaks assigned to surface/bulk dehydroxilation of iron hydroxides (19) and decomposition of surface complexes of CO_2 on iron oxides (20) are observed. It suggest that mechanical activation of α-Fe_2O_3 followed by a contact with atmosphere after drum discharge is accompanied by appearance of the surface carbonates/hydroxides of iron (2+). If this is so, superposition of the surface/bulk reoxidation with a weight loss due to destruction of the surface complexes could be well understood.

Summary of the thermal analysis data. Desorption of chemisorbed carbon dioxide molecules requires at least 10–30 kcal/mole (20), while the heat of iron hydroxides (i.e., goethite) dehydroxilation is around 13 kcal/mole (21). Hence, weight losses in the He stream not accompanied by visible endoeffects imply some exothermic relaxation of defect structure superimposed onto the endoeffects of water and CO_2 removal. Combining the TG data obtained both in He and air, estimation of the degree of sample reduction can be made. For sample activated 15 min it is ca. 0.25 weight%, which corresponds to nearly 1.0% of the anion sublattice. Provided enthalpies of CO_2 and H_2O adsorption are in the range of 10–20 kcal/mole (19, 20), the enthalpy of reoxidation ~(−120–−140) kcal/mole O_2 can be derived. It is rather close to energy required for removal of two oxygen atoms from hematite phase with formation of two anion vacancies and the oxygen molecule (22). Hence, mechanical activation of α-Fe_2O_3 without any new phase formation (vide infra) appears to generate a rather high density of surface/bulk point defects.

Electron Microscopy

1. Initial sample. The particles of the sample are of platelet morphology with rounded or hexagonal contours and typical dimensions ca several thousands Å (Fig. 2). Microdiffraction data show that the most developed faces are of (0001) type (see inset in Fig. 2). Contrast variations are observed at the particles edges as well as on the images of the smaller particles. According to (23), for thin particles these effects can be assigned to some disordering (strains) and/or change of the thickness. Sometimes more bulky aggregates of platelets are encountered.

2. Activated samples. Particles edges are now of layered appearance (steps are clearly visible, Fig. 3), while contrast variations on the particles images are nearly the same as for the initial sample.

XPD

By using diffraction data, crystal structure parameters of the samples were refined; as a typical example, the results obtained for three samples (initial; activated for 15 min; activated for 15 min and then air annealed at 400°C) are listed in Tables 1–3. For comparison, data for the same

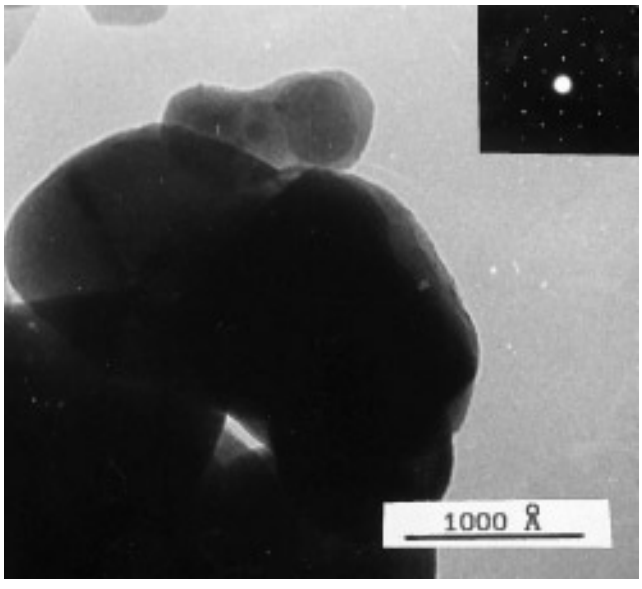

FIG. 2. A typical image of the initial sample particle and corresponding microdiffraction in the ⟨0001⟩ zone.

TABLE 1
Parameters of the Unit Cell and Particle Sizes in the ⟨012⟩ Direction

Sample	a, Å	c, Å	D_{012}, Å
Initial	5.037(1)	13.771(8)	450
Activated 15 min	5.039(1)	13.770(0)	210
Activated 15 min and reoxidized	5.038(2)	13.776(7)	270
Calcined at 800°C	5.032(1)	13.733(4)	>1000
Single crystal data (24, 25)	5.034	13.747	

initial sample but air calcined at 800°C are also included there along with single-crystal data of (24, 25). To facilitate the data analysis, atomic arrangement of the hematite lattice is illustrated in Fig. 4. The crystal structure of hematite is described by the hexagonal $R\bar{3}c$ space group. The iron and oxygen atoms are placed in the (0, 0, z) and (x, 0, $\frac{1}{4}$) positions respectively, where $z = 0.35$ and $x = 0.31$ (24, 25). A numbering of the iron and oxygen atoms in Fig. 4 differs from that used in (24, 25) and aims only at convenience of comparing with the data of Table 3. Oxygen atoms occupy a hexagonal close-packed (hcp) arrangement with $\frac{2}{3}$ of the octahedral positions being occupied by the iron atoms. Along z axis, one empty and two filled octahedrons sharing common face alternate. Due to a mutual repulsion between the neighboring cation layers, cations are shifted from the centers of octahedrons towards the vacant positions. As a result, Fe_1–$O_{1,2,3}$ distances are shorter than those between Fe_1 and $O_{4,5,6}$. Due to a subsequent relaxation in the anion layers, octahedrons in the perfect hematite structure are not ideal: distances between three oxygen atoms forming common face shortened (2.65 Å) while being stretched to the maximum values in the oxygen triangle at the face of an empty octahedron (>3 Å). For the initial sample, Fe–O and O–O distances were found to differ appreciably from the well-known single crystal data (24, 25). Though in the cation layer Fe_1–Fe_2 distances are close to the ideal values, interlayer Fe_1–Fe_3 distances are increased. As a result, unit cell expands along

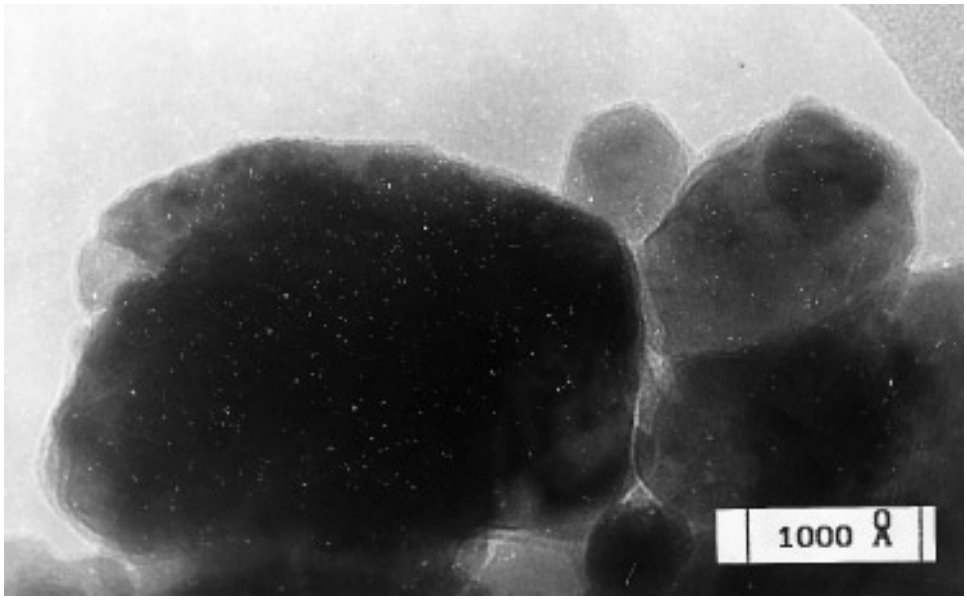

FIG. 3. A typical image of the sample particle activated for 15 min.

TABLE 2
Crystal Structure Refinement Data

Sample	z_{Fe}	Fe occupancy	B_{Fe}, Å^2	x_O	O occupancy	B_O, Å^2	R, %
Initial	0.3557	12	1.0	0.3216	18	1.0	5.3
Activated 15 min	0.3570	12	0.91	0.2973	18	3.0	10.6
Activated 15 min and reoxidized	0.3544	12	0.9	0.3167	18	1.0	6.8
Calcined at 800°C	0.354	12	0.5	0.305	18	0.4	4.5
Single crystal data (25)	0.3553	12		0.303	18		

c axis thus changing the O–O and Fe–O distances. Due to these rearrangements, oxygen octahedron becomes less distorted than in the ideal structure.

Mechanical activation somewhat increases parameter *a*, while the cell length along *c* axis remains unchanged (Table 1). An increase of the B_o parameter for oxygen ions up to 3 Å^2 is also observed (Table 2) evidencing disordering of the anion sublattice. Taken into account the thermal analysis data (vide supra), the latter phenomenon may be assigned to the effect of the anion vacancies generated by activation. Any further refinement (i.e., with a smaller occupation factor for oxygen) is restricted by a rather low reliability of the B_o for powdered samples (±20%). After activation, Fe ions located within doubled octahedra are shifted in the opposite directions approaching the empty interstices, so that Fe_1–Fe_3 distance increases. Oxygen sublattice also rearranges: oxygen anions situated on the face of an empty octahedron become more widely separated while those on the shared face near each other. Therefore the variation of Fe–O distances in the activated sample is explained not only by changes in the distance between cation layers (after activation z_{Fe} increases), but also by relaxation within the anion layer (increase of the difference between O–O distances in the stretched and compressed oxygen triangles, respectively). A driving force for this structure rearrangement seems to be a sample reduction. Indeed, an increase of the Fe cation size and fall of its charge ($r_{Fe^{3+}} = 0.67$ Å; $r_{Fe^{2+}} = 0.80$ Å) is expected to cause repulsion (or at least weaken interaction) between the layers due to steric as well as electrostatic effects, while appearance of the vacancies helps anion layers to relax into a new configuration. As a result, after activation O–O distances approach those typical for the nearly perfect high-temperature sample, though interlayer Fe_1–Fe_3 distance deviates further from the ideal value.

Mild reoxidation at 400°C has appreciably affected the atomic arrangement (Table 3). Clearly, a structure parameters relaxation after reoxidation is caused by incorporation of oxygen into the anion sublattice, thus filling vacancies (parameter B_o returns to the initial value). Reoxidation is also accompanied by a decrease in the Fe_1–Fe_3 distance attaining the ideal value (2.87 Å), while O–O distances nearly regain their original values. Therefore, in the reoxidized sample the situation is quite opposite to that in the activated: cation interlayer distances are close to the ideal values, while O–O distances deviate essentially from the values typical for high-temperature samples. It means that in the reoxidized sample relaxations in the anion sublattice are not determined by shift of the cation layers. The data of the Table 3 show that in the reoxidized sample the

TABLE 3
Interatomic Distances in the Hematite Samples

	Sample				
Type of distance, Å	Initial	Activated 15 min	Activated 15 min and reoxidized	Calcined at 800°C	Single crystal data (24, 25)
Fe_1–$O_{1,2,3}$	1.90	1.96	1.92	1.95	1.9511
Fe_1–$O_{4,5,6}$	2.18	2.10	2.14	2.10	2.1028
O_1–$O_{2,3}$	2.96	3.08	2.98	3.04	3.0472
O_1–O_4	2.86	2.90	2.87	2.89	2.8887
O_1–O_5	2.81	2.76	2.80	2.77	2.7651
O_4–$O_{5,6}$	2.81	2.60	2.76	2.65	2.6419
Fe_1–Fe_2	2.97	2.98	2.97	2.97	2.9685
Fe_1–Fe_3	2.91	2.95	2.87	2.87	2.8951

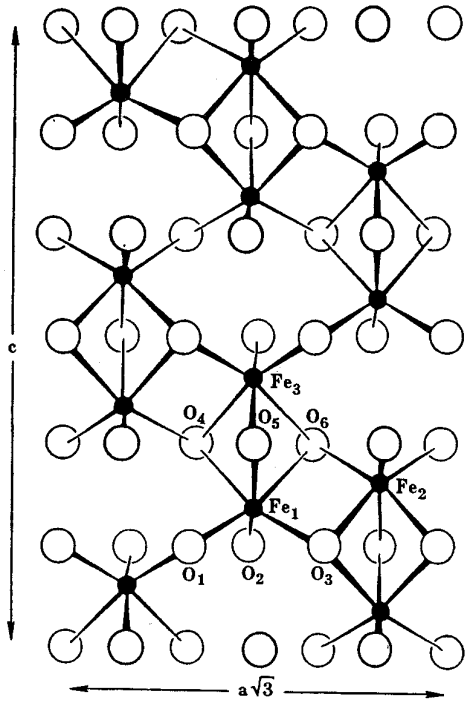

FIG. 4. Atomic arrangement of the hematite lattice in the [1120] projection.

empty octahedra are more compressed than it should be for the ideal structure while shared face in the filled octahedra is somewhat stretched. Such effect may be assigned to a partial occupation of the empty interstices by admixed sodium cations which are expected to prefer these larger octahedra due to their rather big sizes ($r_{Na^+} = 0.95 - 1.01$ Å). Moreover, after activation with subsequent reoxidation a part of Fe cations can be transferred into these interstitial positions via cooperative displacements (vide infra) forming a cation stacking fault (10). Indeed, some decline of the *R*-factor value was obtained when placing ca. 1% of Fe atoms in these positions not occupied in the ideal hematite structure. Such filling of the usually vacant positions is expected to cause the same type of relaxation as observed: stretching of the O_{4-6} and compressing the O_{1-3} triangles.

To calculate particles sizes and microstrains densities, a pair of the (012) and (024) diffraction peaks was analyzed. The ratio of the halfwidths of these peaks was found to correspond to the reciprocal ratio of cosines of the reflection angles. It means that broadening of the diffraction peaks is mainly caused by the size effect while microstrains are absent. The values of the particles sizes calculated for 15 min activated sample are given in Table 1. As follows from these results, some decrease of the sizes is observed that correlates with increase of the specific surface. However, a simple estimation shows that at such typical particles' sizes provided platelet form is retained, specific surface values must be ca. 40–60 m^2/g, that is, 2–3 times higher than the measured ones (ca. 20 m^2/g). Hence, some particles appear to be composed from smaller ones with those typical sizes.

IR Spectroscopy of Lattice Vibrations

A spectrum of the initial sample (Fig. 5, curve 1) resembles those of the low-temperature samples prepared from goethite (8): absorption bands are shifted to lower frequencies as compared with positions for the high-tempera-

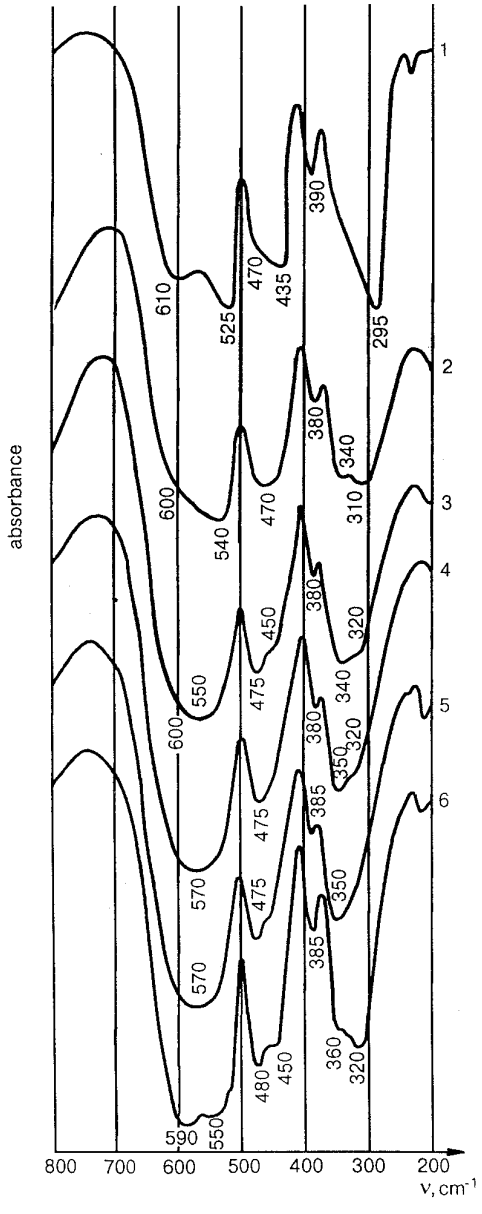

FIG. 5. IR-spectra of the initial (1) and activated for 1 min (2), 5 min (3), 10 min (4), and 15 min (5) samples of hematite. (6) The sample activated for 15 min was reoxidized at 400 C for 1h.

TABLE 4
Integral Intensity of SAXS and Reactivity of Hematite Samples as Functions of the Time of Activation

				Reaction rate, 10^{16} molecules CO/m^2sec[a]					
		I SASX, rel. units.		Treatment 1			Treatment 2		
Time of activation, min	Specific surface, m^2/g	as received	after Treat.2	140i	140ss	227ss	227i	227ss	140ss
0	14	278	—	2.3	0.32	4.0	32	10.7	0.71
1	22	201	—	1.8	0.29	3.0	11	4.2	—
2	23	148	79	1.1	0.22	2.5	7.2	3.6	0.17
5	24	142	75	0.62	0.14	2.8	6.2	1.8	—
10	23	143	—	0.62	0.23	2.0	1.6	—	—
15	21	107	—	0.26	0.09	—	1.0	0.43	—

[a] i, initial activity; ss, steady-state activity.

ture samples (339 $cm^{-1} \rightarrow$ 295 cm^{-1}; 470 $cm^{-1} \rightarrow$ 435 cm^{-1}; 545 $cm^{-1} \rightarrow$ 525 cm^{-1}; 630 $cm^{-1} \rightarrow$ 610 cm^{-1}.

Some noticeable variations in the spectra appear even after first 5 min of activation (Fig. 5, curve 2): new components emerge at ~340 and 470 cm^{-1}, while band situated at ~610 cm^{-1} actually disappears. The first two bands are situated at positions typical for the α-Fe_2O_3 high temperature samples with a rather perfect hematite structure. Hence, at first stage of activation a spectrum can be described as a superposition of those for the untapped and activated particles.

As activation proceeds further (up to 15 min), positions of the low-frequency bands at 230, 350, and 380 cm^{-1} (Fig. 5, curve 5) became nearly identical with those for the high-temperature samples studied in (8). Nevertheless, for high-frequency bands situation is somewhat different. Namely, for the ideal hematite structure bands situated at 470 and 545 cm^{-1} are rather narrow with a shoulder at 630 cm^{-1} (8). For 15 min activated sample, components situated at ~480 and 570 cm^{-1} are rather broad while shoulder at 630 cm^{-1} is not observed. Hence, after activation a structure of the samples studied here only partially approaches that for the perfect hematite. A similar trend was observed by XPD: after activation only a part of the interatomic distances relax to the ideal values (Table 3).

In a similar way, air reoxidation at 400°C of the 15 min activated sample makes spectrum a mixture of those for the initial and activated parts that agrees well with the observed by XPD changes of the interatomic distances (vide supra).

X-Ray Small Angle Scattering

Integral intensities of scattering on the extended regions of a distorted structure (typical dimensions less than 200 Å) are given in Table 4. Usually, regions with a changed electron density having such typical dimensions are assigned to dislocations, stacking faults, etc. (4). As evident from the Table 4, mechanical activation is accompanied by a decline in the density of such extended defects. Further intensity decline is caused by a mild reoxidation of the activated samples.

Magnetic Susceptibility Measurements

At room temperature, α-Fe_2O_3 is known to be a weakly ferromagnetic compound (parasitic ferromagnetism (26)) with low magnetic susceptibility (ca. 10^{-5} emu) independent upon the applied magnetic field. Spinel γ-Fe_2O_3 is a strong ferrimagnetic with high value of the room-temperature saturated magnetization ($\sigma_{298} \sim 95$) (27, 28). Hence, even small admixtures of spinel phase in hematite can easily be detected by magnetic methods.

As apparent from the data of Table 5, the initial sample contains some admixture of spinel phase diminishing in the course of mechanical activation. Since mechanical activation is also accompanied by the extended defects density fall (vide supra), fragments with spinel structure are more likely to exist rather as extended defects (grain boundaries, anion stacking faults, microinclusions) than a mechanical

TABLE 5
Magnetic Data

Sample	Magnetization, σ_{3700}[a]	Gs cm^3/g σ_{7400}[a]	% of γ-Fe_3O_3
1. Initial	1.24	1.37	1.3
2. Activated 10 min	0.38	0.47	0.3
3. Activated 15 min	0.30	0.39	0.23
4. Hematite from goethite calcined at 700°C	0.06	0.12	—
5. Sample N4 reduced by CO pulses	0.62	0.73	0.6

[a] Magnetization at 3700 and 7400 Oe, respectively.

TABLE 6
Relative Surface and Bulk Concentrations of Elements by SIMS

Sample	Sputtering depth, Å	Relative concentrations of elements, %				
		C	O	Na	Al	Fe
Initial	0	0.8	60	0.9	0.3	38.0
	100	0.3	60.6	0.05	0.15	38.2
Activated 15 min	0	1.1	44	1.0	1.7	52.2
	100	0.6	53.1	0.15	0.6	45.2
Activated 15 min and reoxidized at 400°C	0	2.1	57.7	0.8	1.2	38.2
	100	0.8	58.4	0.06	0.25	40.4

admixture. Taken into account the XPD and EM data, such defects appear to be mainly located in the near-surface layer of the particles. However, very small spinel particles are rather expected to be superparamagnetic (29). To check whether spinel microparticles embedded into the surface layer of a weakly ferromagnetic α-Fe_2O_3 can also be ferromagnetic, a sample from the goethite series (9) without any ferrimagnetic admixtures was reduced by pulses of 1% CO in He at 227°C removing ca. 30% of the oxygen monolayer (1 monolayer = 10^{19} atoms/m^2) and was cooled in He to room temperature and its magnetic properties were studied. In such a way spinel clusters (nuclei) at outlets of extended defects are mainly expected to be formed (15). For this sample before reduction, the density of the surface defect centers could be roughly estimated as being around 1–2% of a monolayer (9, 15). Hence, after reduction spinel clusters including ca. 20–30 Fe^{2+} ions might appear. As follows from the data of Table 5, in our case such small clusters are indeed ferromagnetic. A typical sizes of such domains should be ca. 30–40 Å to have room-temperature ferromagnetic properties (28) rather close to our estimations. Hence, existence of similar ferromagnetic domains on the surface of the initial sample seems to be quite probable. Some influence of the weakly ferromagnetic α-Fe_2O_3 matrix on the spin ordering in these domains might also be expected, though any detailed discussion of this question is clearly beyond the scope of this paper.

Secondary Ions Mass Spectroscopy

The data for initial, activated for 15 min, and annealed samples are given in Table 6. The most apparent result is the surface and bulk reduction of the activated sample, the surface being more reduced. Subsequent reoxidation at 400°C nearly restores the initial sample stoichiometry. Base metal admixtures such as Na and Al brought from the starting compound (ammonium oxalatoferriate) appear to be only minor impurities not capable thus to block surface sites. However, strong tendency for sodium accumulation in the surface and near-surface layers deserves attention. Since the alkali metal ions are known to stabilize a spinel structure, the relative stability of the residual γ-phase fragments on the surface may be explained by this effect. Some tendency for Al accumulation on the surface due to activation can also be inferred, explained, perhaps, by some transfer from the corundum drum and balls.

Infrared Spectroscopy

IR-spectra of surface OH-groups are given in Fig. 6. For initial sample, two bands situated at 3660 and 3515 cm^{-1} are clearly observed. The first one is usually assigned to isolated surface OH-groups (free terminal OH-band) (17). According to Busca *et al.* (30), the existence of such OH-groups on the surface of α-Fe_2O_3 particles with predominantly developed (0001) plane gives evidence that maghemite (γ-Fe_2O_3) rafts are present due to a rearrangement of the oxygen atoms in the outer layer from the normal hcp structure to alternative ccp positions. The lower frequency absorption (3515 cm^{-1}) corresponds to an O–H···O hy-

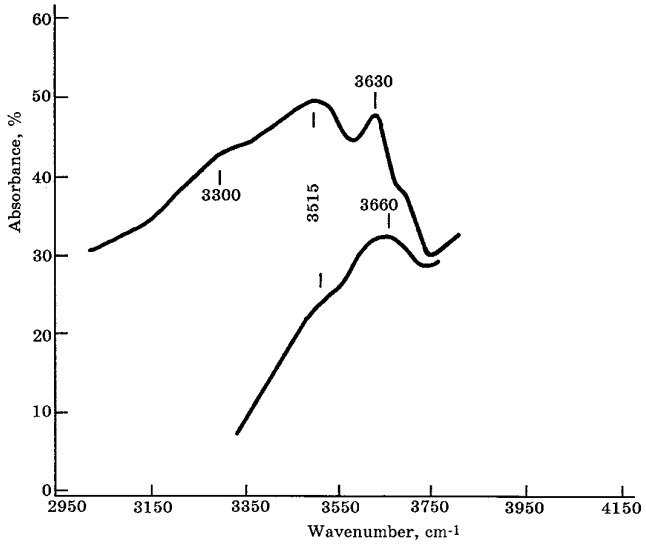

FIG. 6. IR spectra of surface OH-groups. 1, initial sample; 2, sample activated for 15 min.

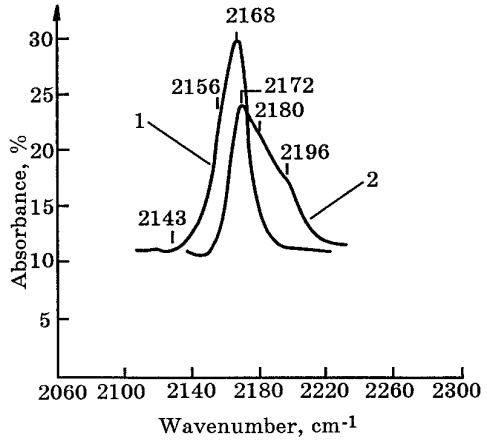

FIG. 7. IR-spectra of adsorbed CO: 1, initial sample; 2, sample activated for 15 min.

drogen bonded OH in open cavities of the surface or in micropores (30–32).

The spectrum of activated sample is rather different. Additional intense bands at 3630 and 3300 cm^{-1} appear while intensity of the 3515 cm^{-1} absorption band appreciably enhances. Narrow band at 3630 cm^{-1} is assigned to bridged OH's of the hcp surface structure (33), while the band at 3300 cm^{-1} may be due to more strongly H-bonded OH-groups (17). A pronounced increase in the number of hydrogen-bonded hydroxyls in the course of activation is well manifested. More subtle changes appear to be associated with decline in the number of terminal OH-groups on ''maghemite'' rafts.

IR-spectra of adsorbed CO. Figure 7 demonstrates the spectra of CO adsorbed on the surface of the initial and activated samples. An intense band situated at 2168 cm^{-1} clearly dominates in the former case. Analysis of the absorption band contour by a procedure described in (17) also reveals weak absorption at 2156 cm^{-1}. Hence, centers of CO adsorption, coordinatively unsaturated Fe cations, are rather uniform. Earlier (15) such centers forming CO complexes with νCO $\sim$ 2170 cm^{-1} were proved to be clusters of Fe^{2+} ions probably located at outlets of the extended defects.

Mechanical activation drastically changes the appearance of the spectrum: a high-frequency band emerges at 2196 cm^{-1} while the intensity of the $\sim$2170 cm^{-1} band declines. Mathematical analysis reveals also a band at $\sim$2180 cm^{-1}. By analogy with (34), the high-frequency band can be assigned to CO complexes, with Fe cations having a higher degree of coordinative unsaturation. Moreover, assignment of the band at 2196 cm^{-1} to isolated Fe^{3+}–CO complexes seems quite probable. In every case, CO complexes with isolated highly charged ions are known to have higher frequencies than those with clustered ions (35). Hence, we have a rather strong reason to suggest that mechanical activation followed by thermal annealing causes dissociation of the extended surface defects (clusters) into smaller ones (pairs, etc. manifested in the shift of the 2170 cm^{-1} absorption band to 2180 cm^{-1}) or even into isolated coordinatively unsaturated (cus) cations. Moreover, after activation only $\sim$ half of cus Fe ions capable to retain CO at room temperature remains on the surface.

Catalytic Activity

Standard pretreatment is a necessary preliminary procedure before measuring the rates of carbon monoxide oxidation catalyzed by oxides. The aim of this procedure is to clean the surface from adsorbed water, organic residues and carbonates as well as to level off the surface stoichiometry and degree of hydroxylation. Usually pretreatment temperatures are $\sim$400°C. However, in our case we have to take into account the disappearance of point defects at temperatures ca. 300°C (vide supra). Hence, two temperatures of pretreatment (227 and 400°C successively) were chosen to discriminate the influence of point and extended defects on activity. To evaluate also the role of defects which could be easily annealed or blocked in the reaction media, both initial (in the first pulse of reaction mixture) and steady-state (in the flow of reaction mixture) activities were determined.

The results obtained are given in Table 4. For all pretreatments and conditions of activity measurements, ball milling appear to deactivate our hematite sample. Since activity decline is accompanied by accumulation of both bulk and surface point defects (anion vacancies, isolated coordinatively unsaturated cations, vide supra), we can suggest that these defects are not the active centers. On the contrary, there is some reasonable correlation of activity with the density of extended (clustered) defects determined by using XSAS and IR-Spectroscopy of adsorbed CO (Table 4, Fig. 7). So surface clusters of coordinatively unsaturated cations are good candidates for the active centers. Some less evident conclusions can be drawn by taking into account the variation of the degree of surface hydroxylation with the temperature of pretreatment. Thus, for the initial sample, the increase of the pretreatment temperature from 227 to 400°C is accompanied by a pronounced increase of the steady-state activity at both 140 and 227°C. At the same time, for activated samples, there is either a less pronounced increase on even some decline in activity at higher activation temperatures. Hence, decline in the density of extended defects after reoxidation (see Table 4) is reflected in the fall in sample reactivity.

Some comments can also be made about the possible effect of the oxygen octahedra distortions on the hematite reactivity. Though reoxidation of the activated samples restores distortions partially eliminated by mechanical acti-

vation (vide supra), activity declines. Hence, such distortions seem to be of no importance for reactivity.

Last, a question about the role of γ-phase admixture deserves special discussion. Some speculation might be possible assigning enhanced activity of the initial sample to purely additive effects if the specific activity of the spinel phase is higher than that of hematite. Though this problem will be considered more thoroughly in a separate publication, rather low activity of γ-Fe_2O_3 found here ($5 \cdot 10^{15}$ molecules CO/m^2s; steady state at 227°C, treatment 1) is not in favor of such ideas.

DISCUSSION

Cooperative Distortions of Hematite Structure and Mechanical Activation

Cooperative distortions of the lattice (including modulated structures) are among the most intensively studied topics in modern solid state chemistry and crystallography (36–41). The data obtained in this work together with our earlier results (8, 9) demonstrate that for corundum-type structures cooperative distortions caused by impurities are rather typical features of the low-temperature samples. In particular, a long-discussed problem of the specific spectral appearance of hematite samples prepared from goethite (8, 42–44) is directly relevant to these effects. Serna and Iglesias (42) earlier assigned shift and splitting of some absorption bands to surface modes domination in the spectrum, needle-like particle morphology being of crucial importance. The other hypothesis tends to explain these features by intermediate formation of some low-temperature phases (protohematite or hydrohematite) stabilized by the residual lattice hydroxyls (8, 43–44). Both hypotheses appear not to be applicable to samples studied here since their particles are of platelet morphology and no lattice hydroxyls were found by thermal analysis. At the same time, there is a strong similarity of the variation of interatomic distances in the samples considered here to that in the low-temperature samples prepared from goethite (9). For the latter samples, this effect was explained by the location of protons within the anion layers decreasing the effective charge of the anion layers and the strength of their interaction with cation layers. Due to the increasing interlayer distances, oxygen anions forming shared faces in the filled octahedra are pushed aside, increasing the O–O distance in this triangle. For the samples considered in this work, sodium ions can play the same role as protons. From the microscopic point of view, each admixed cation can distort only one or two octahedra. To produce any change of the lattice parameters, cooperative elastic effects should operate to cause spatial ordering of the distorted octahedra (41).

In general, cooperative displacements of the atoms and change of the interatomic distances in the corundum-type structure can occur without reduction in the space group symmetry, since relaxation within the anion layers, as well as shift of the iron atoms along the z-axis, preserves centers of inversion in the doubled occupied octahedra. However, IR data (especially the appearance of new absorption bands) are in favor of some variation in the octahedron symmetry. It might be generated by some shift of anions along the z axis, which is forbidden within the $R\bar{3}c$ space group but is rather possible in lattices somewhat distorted by impurities.

In the framework of the scheme considered above, the mode of the deformation of octahedra is determined primarily by the distance between the cation layers. Nevertheless, some correlation in the spatial distribution of admixed cations either located within interstitial positions (Na^+, Fe^{3+}) or included into the anion layers (H^+) and thus able to affect relaxation within the anion sublattice seems also to be of importance. Indeed, in the case of a hematite prepared from an amorphous hydroxide where no such correlation in the distribution of hydroxyls is expected, specific spectral features of the type discussed here were not observed (8).

Point and Extended Defects

Oxide reduction in the course of mechanical activation under inert atmospheres is a well-known fact, especially when steel balls are used (45). However, for hematite, only the transition into spinel Fe_3O_4 was well documented (46). Air activation of coarse-powdered hematites was found to generate stacking faults and residual microstrains (47). Fine-powdered hematites subjected to shear deformation under high pressure on a Bridgeman anvil developed only a dislocation network with dislocations lying in the basal plane (48). Hence, the generation of anion vacancies in hematite by mechanical activation demonstrated here is a unique finding deserving thorough consideration. Moreover, accompanying this phenomenon, a decline in the density of extended defects is also rather unexpected. It is quite clear that any explanation has to be sought both in the peculiarities of the initial defect structure/morphology of the sample and in the mechanism of corundum-type structure deformation.

The results obtained there permit the inference that for the initial sample the predominant types of extended defects are surface or subsurface defects (anion stacking faults, etc.) with local arrangements of spinel type. These defects are the remnants of the precursor γ-phase after complete transformation of the cubic closest packed anion sublattice (ccp) into the hexagonal one (hcp) via consecutive shift of the oxygen layers (49). Since surface defects with a local spinel structure were also found to persist after complete bulk transformation of a γ-alumina into the nearly perfect α-alumina (50, 51), these results seem to be of general significance for oxides with hcp anion sublattices.

In contrary to the case of goethite–hematite topotactical transformation accompanied by generation of a great number of bulk extended defects (twins, stacking faults) (9), thin spinel particle rearrangement occurs without accumulation of bulk defects. Possibly, in the former case, relative stability of bulk extended defects can be assigned to residual lattice hydroxyls somewhat decreasing electrostatic repulsion between sheared anion layers. For samples considered in this work relative stability of the surface defects may be explained by a preferential near-surface location of the sodium ions.

Due to the platelet morphology of the particles with the most developed basal planes, a rather high density of surface defect centers is achieved though the number of misplaced iron atoms in the particle is small. Another important consequence of this morphology is that the basal plane is expected to contact preferably with the milling balls. Some decrease of the particle sizes (XPD) and appearance of steps on the side faces without dislocation generation in the bulk (TEM) are in favor of the slip in the basal plane. This agrees well with the theoretical analysis of Kronberg (10). Earlier Pavlukhin *et al.* (52) have also observed slip along the (111) densely packed plane in spinels in the course of mechanical activation. It was accompanied by a shift of cations from tetrahedra into larger octahedra. The same process appears to operate in our case since decline of magnetic susceptibility after activation indicates a decrease in the number of Fe ions in tetrahedra bound with residual anion stacking faults. This result appears to be expected since the anion stacking fault is the most unfavorable by energy (10). Probably, the decrease of the particle sizes and the appearance of steps after activation indicate the generation of low-energy cation stacking faults (10) or glide twins (12) in whose vicinity iron atoms are shifted into interstitial positions.

Some ideas about the mechanism of point defect generation can also be formulated. According to dislocations theory, the most probable route to the generation of point defects by plastic deformation is via annihilation of two dislocations lying in the neighboring slip planes and having opposite signs of Burgers vectors (26). In our sample, the particles' thickness in the $\langle 0001 \rangle$ direction is quite small; hence the distance between such dislocations has to be small, thus ensuring a high probability of their annihilation. A very important consequence from Kronberg analysis (10) is associated with the requirement of cooperative displacement of both cations and anions. This means that self-pinning occurs if either kind of ions is unable to move. It seems that in our case dislocations are pinned by anion vacancies disturbing this cooperative displacement. If this is so, at some critical concentration of vacancies plastic deformation of hematite is hindered. Rather, further supply of energy results in additional generation of point defects and, finally, in sample amorphization. The absence of any extended defect accumulation in our sample as activation proceeds, as well as the invariable morphology of particles, is in agreement with this supposition. Nevertheless, this scheme of anion vacancy generation is purely phenomenological and requires some further microscopic refinement.

In a similar way, decrease in the extended defect density after reoxidation can be formally assigned to a well-known mechanism of dislocation climb (thus dislocation escapes from the crystal) (26).

Catalytic Activity/Reactivity and Mechanical Activation

In the temperature range studied, catalytic oxidation of carbon monoxide on hematite is described by the reduction–reoxidation scheme, and the rate of catalysis is determined by (and is equal to) the rate of carbon monoxide interaction with reactive surface oxygen (54). Reoxidation of reduced centers was found to proceed much faster and thus to be non-rate-determining (55). Hence, in the same state of the surface (first of all, stoichiometry), the rate of catalytic reaction is the measure of sample reactivity determined by the density of surface active centers and by the strength of oxygen bonding with these centers.

The fall of oxide systems reactivity under the effect of mechanical activation is not a common phenomenon though previously observed for such system as Co_3O_4 (56). In our case the decreased density of surface cluster defects due to activation is able to explain this fact. From the point of view of the atomic structure of surface active centers, several facts deserve special comment.

(1) Isolated coordinatively unsaturated Fe ions located on the most developed basal planes (surface point defects) were proved not to have any increased reactivity. Possible models of such defects were considered in (57, 58). The perfect basal plane (10) appears to be covered by oxygen that is tightly bound with two cations and thus nonreactive.

The simplest point defect in the basal plane, anion vacancy, generates two coordinatively unsaturated (cus) surface cations. Isolated cus surface cations can appear if one of cations is blocked by the OH-group. Low reactivity of isolated centers appear to stem primarily from the difficulty of dissociating molecular oxygen (two vacancies for two oxygen atoms are required). In every case, stability of these centers to oxidative treatment means that they are not capable of coordinating any forms of oxygen and thus cannot take part in the redox catalytic cycle.

(2) Reactive surface cluster centers appear to include Fe cations in coordination other than octahedral (distorted tetrahedral). An increased reactivity of the surface oxygen forms bound with cluster centers was found to be a rather common feature for transition metal oxides (4, 5, 59). The most reactive forms are located on the centers where surface cation in truncated octahedra is bound with subsurface

interstitial cation in distorted tetrahedra. In this case some metal–metal bond between these cations appears whose strengthening in the course of *Me*–O bond rupture facilitates oxygen removal (59). A more detailed analysis of the surface centers' structures bound with various types of defects and situated at various surface faces, together with calculations of the oxygen adsorption heats by semiempirical interacting bond methods, will be given in a separate paper (50).

ACKNOWLEDGMENTS

We are thankful to Dr. G. N. Kryukova for providing TEM data. This work is in part supported by International Science Foundation Grant RPV000.

REFERENCES

1. L. C. Dufour, *in* "Non-Stoichiometric Compounds. Surfaces, Grain Boundaries and Structural Defects" (J. Novotny and W. Wepner, Eds.), NATO ASI Series, Series C: Mat. and Phys. Sci., Vol. 276, p. 311. Kluwer Academic, Dordrecht/Boston/London, 1989.
2. Pr. L. Gai-Boyes, *Catal. Rev. Sci. Eng.* **34,** 1 (1992).
3. V. D. Berg, A. J. V. Dillen, and J. V. D. Meiden, *in* "Surface Properties and Catalysis by Non-Metals, 1983" (J. Novotny, Ed.), p. 493.
4. V. A. Sadykov, S. F. Tikhov, G. N. Kryukova, N. N. Bulgakov, V. V. Popovskii, and V. N. Kolomiichuk, *J. Solid State Chem.* **74,** 200 (1982).
5. G. N. Kryukova, A. L. Chuvilin, and V. A. Sadykov, *J. Solid State Chem.* **89,** 208 (1990).
6. V. I. Kuznetsov, V. A. Sadykov, V. A. Razdobarov, and A. G. Klimenko, *J. Solid State Chem.* **104,** 412 (1993).
7. Yu. A. Lokhov, S. F. Tikhov, M. N. Bredikhin, A. G. Zhirnyagin, and V. A. Sadykov, *Mend. Commun.* **1,** 10 (1992).
8. G. N. Kustova, E. B. Burgina, V. A. Sadykov, and S. G. Poryvaev, *Phys. Chem. Miner.* **18,** 379 (1992).
9. G. N. Kryukova, S. V. Tsybulya, L. P. Solovyeva, V. A. Sadykov, G. S. Litvak, and M. P. Andrianova, *Mater. Sci. Eng. A* **149,** 121 (1991).
10. M. L. Kronberg, *Acta Metallurg.* **5,** 507 (1957).
11. J. Hornstra, *Phys. Chem. Solids* **15,** 311 (1960).
12. L. A. Bursill and R. L. Wither, *Phil. Mag. A* **40,** 213 (1979).
13. L. A. Isupova, V. Yu. Alexandrov, V. V. Popovskii, V. A. Balashov, A. A. Davydov, A. A. Budneva, and G. N. Kryukova, *React. Kinet. Catal. Lett.* **31,** 195 (1986).
14. V. A. Sadykov, S. F. Tikhov, and V. A. Razdobarov, *in* "Unsteady-State Processes in Catalysis: Proceedings, I International Conference, Novosibirsk, Elsevier, 1990" (Yu. Sh. Matros, Ed.), p. 407.
15. S. F. Tikhov, V. A. Sadykov, G. N. Kryukova, and V. A. Razdobarov, *Mend. Comm.* **1,** 69 (1994).
16. S. V. Tsybulya, S. V. Cherepanova, A. V. Ovchinnikov, and L. P. Solovyeva, *in* International Conference, Powder Diffraction and Crystal Chemistry, Saint Petersburg, 1994, Collected Abstracts," p. 24.
17. E. A. Paukshtis, "IR-Spectroscopy in Heterogeneous Acid–Base Catalysis," Nauka, Novosibirsk, 1992.
18. F. Van der Droude, *Phys. Status Solidi* **17,** 417 (1966).
19. E. Patterson and R. Swaffield, *J. Therm. Anal.* **18,** 161 (1980).
20. T. J. Udovic and J. A. Dumesic, *J. Catal.* **89,** 314 (1984).
21. M. V. Borisov, and Yu. B. Shvarov, "Thermodynamics of Geochemical Processes," Moscow State Univ., Moscow, 1992. [In Russian]
22. G. I. Golodets, Yu. I. Pyatnitskii, and V. V. Goncharuk, *Teor. Exp. Khim* **4,** 53 (1968). [In Russian]
23. L. D. Marks, *Surf. Sci.* **150,** 302 (1985).
24. R. L. Blake, R. E. Hessevic, T. Zoltai, and L. W. Finger, *Am. Mineral.* **51,** 123 (1966).
25. L. W. Finger and R. M. Hasen, *J. Appl. Phys.* **51,** 5362 (1980).
26. R. Kubo, and T. Nagamura, "Solid State Physics," McGraw–Hill, New York, 1969.
27. G. Bate, *in* "Ferromagnetic Materials" (E. P. Wohlfarth, Ed.), Vol. 2, p. 443, 1980.
28. P. W. Selwood, "Magnetochemistry." Interscience, New York, 1956.
29. J. H. Coey and D. Khalafalla, *Phys. Status Solidi A* **11,** 229 (1972).
30. G. Busca and V. Lorenzelli, *React. Kinet. Catal. Lett.* **15,** 273 (1980).
31. C. N. Rochester and S. A. Topham, *J. Chem. Soc. Faraday Trans. 1* **75,** 591, 1073, 1259 (1979).
32. C. Morterra, G. Ghiotti, E. Garrone, and F. Boccuzzi, *J. Chem. Soc. Farad Trans. 1* **72,** 2722 (1976).
33. A. A. Tsyganenko and N. N. Filimonov, *Spectrosc. Lett.* **5,** 477 (1972).
34. A. A. Davydov, "Infra-Red Spectroscopy of Adsorbed Species on the Surface of Transition Metal Oxides," p. 243. Wiley, Chichester/New York, 1990.
35. R. I. Soltanov, E. A. Paukshtis, E. N. Yurchenko, B. A. Dadashev, S. E. Mamedov, and B. A. Gasymov, *Kinet. Katal.* **25,** 729 (1984). [In Russian]
36. J. S. Anderson, *in* "Modern Aspects of Solid State Chemistry" (C. N. R. Rao, Ed.). Plenum, New York, 1970.
37. C. N. R. Rao, J. Gopalakrishnan, and K. Vidysagar, *Ind. J. Chem. A* **23,** 265 (1984).
38. J. Smith, J. Yeomans, and V. Heine, *in* "Proceedings, NATO Advanced Studies Institute on Modulated Structure Materials" (Tsakalakos, Ed.), p. 95. Nijhoff, Dordrecht, 1984.
39. J. B. Goodenough, *J. Solid State Chem.* **12,** 148 (1975).
40. B. C. Tofield and W. B. Scott, *J. Solid State Chem.* **10,** 183 (1974).
41. D. Reinen, *J. Solid State Chem.* **27,** 71 (1989).
42. C. J. Serna and J. E. Iglesias, *J. Mater. Sci.* **5,** 901 (1986).
43. E. Wolska and W. Szajda, *J. Mater. Sci.* **20,** 4407 (1985).
44. Sh. Yariv and E. Mendelovici, *Appl. Spectrosc.* **33,** 410 (1979).
45. E. G. Avvakumov, "Mechanical Methods of Chemical Processes Activation." Nauka, Novosibirsk, 1986. [In Russian]
46. E. G. Avvakumov, A. F. Krechman, and T. L. Marks, *Izv. Sib. Otd. Akad. Nauk SSSR Ser. Khim. Nauk* **4,** 3 (1977).
47. L. A. Panchenko, Thesis, Moscow State Univ., 1982.
48. O. S. Morozova, Yu. I. Maksimov, D. P. Shashkin, P. A. Shirjaev, V. V. Matveev, V. A. Zhorin, O. V. Krylov, and G. N. Kryukova, *Appl. Catal.* **78,** 227 (1991).
49. S. Kachi, K. Motiyama, and Sh. Shimizu, *J. Phys. Soc. Jpn.* **18,** 106 (1963).
50. C. Morterra, G. Ghiotti, E. Garrone, and F. Boccuzzi, *J. Chem. Soc. Faraday Trans 1* **72,** 2722 (1976).
51. C. Morterra, S. Coluccia, A. Chiorono, and F. Boccuzzi, *J. Catal.* **54,** 348 (1978).
52. Y. T. Pavlukhin, Ya. Ya Medikov, and V. V. Boldyrev, *J. Solid State Chem.* **53,** 155 (1984).
53. H. Hoshino and N. L. Peterson, *J. Phys. Chem. Solids* **46,** 1247 (1985).
54. V. A. Razdobarov, Thesis, Boreskov Institute of Catalysis, Novosibirsk, 1992.
55. A. Ya. Rozovskii, "Catalysts and Reaction Media," Nauka, Moscow, 1988.
56. L. A. Isupova, Thesis, Boreskov Institute of Catalysis, Novosibirsk, 1989.
57. D. Scarano, A. Zecchina, and A. Peller, *Surf. Sci.* **198,** 11 (1988).
58. A. Zecchina, D. Scarano, and A. Peller, *J. Chem. Soc. Faraday Trans. 1* **84,** 2327 (1988).
59. V. A. Razdobarov, V. A. Sadykov, S. A. Veniaminov, N. N. Bulgakov, O. N. Kovalenko, Yu. D. Pankratiev, V. V. Popovskii, G. N. Kryukova, and S. F. Tikhov, *React. Kinet. Catal. Lett.* **37,** 109 (1988).
60. N. N. Bulgakov and V. A. Sadykov, submitted for publication.